J|A|C|S ARTICLES

Published on Web 03/30/2010

Formation of Beyerene, Kaurene, Trachylobane, and Atiserene Diterpenes by Rearrangements That Avoid Secondary Carbocations

Young J. Hong and Dean J. Tantillo*

Department of Chemistry, University of California, Davis, One Shields Avenue, Davis, California 95616

Received October 5, 2009; E-mail: tantillo@chem.ucdavis.edu

Abstract: Quantum chemical calculations on carbocation intermediates encountered during the conversion of *ent*-copalyl diphosphate to the diterpenes beyerene, kaurene, trachylobane, and atiserene are described. Based on the results of these computations, it is suggested that previously proposed secondary carbocation intermediates are avoided. In some cases, complex rearrangements in which up to three alkyl or hydride shifting events are coupled into concerted processes are predicted to occur instead. The potential effects of electron-rich active site groups on the inherent reactivity of key carbocations are discussed, as are complex rearrangements coupled to deprotonation events. Based on computed electrostatic potential maps, it also is proposed that ammonium ions that were previously designed as mimics of several carbocations are actually better mimics of transition state structures for carbocation deprotonation.

Introduction

Enzyme-mediated carbocationic rearrangement is a key process by which Nature manufactures complex polycyclic terpenes.[1] For example, such processes generate a diverse array of polycyclic diterpene natural products from a single substrate (GGPP, **1**, Scheme 1).[2−4] Interestingly, these pathways combine two types of enzyme-triggered carbocation rearrangements: those triggered by protonation (to form copalyl diphosphate (CPP) and related decalin derivatives) and those triggered by pyrophosphate removal (to form the various diterpenes highlighted in Scheme 1). We focus herein on the latter. We have previously discussed the formation of abietadiene (**6**), which is derived from CPP (Scheme 1).[5−7] Here we focus on the formation of polycyclic diterpenes derived from *ent*-CPP (**2**−**5**, Scheme 1). *Ent*-beyerene (**2**), *ent*-kaurene (**3**), *ent*-trachylobane (**4**), and *ent*-atiserene (**5**) are widespread in plants where, for example, *ent*-kaurene is a precursor to the gibberellin phytohormones (for simplicity, and since enantiomers will, by definition, have identical energies in the absence of a chiral environment, we refer to all structures discussed from here onward without "*ent*" labels).[2−4,8]

The enzyme-catalyzed formation of diterpenes **2**−**5** is usually proposed to proceed via the reaction mechanism shown in Scheme 1 (or something very similar).[2b,9] The generation of the pimarenyl carbocation (**A**, Scheme 1), upon loss of pyrophosphate from *ent*-CPP and cyclization (either in a concerted or stepwise fashion), precedes a series of rearrangement and cyclization events. The pimarenyl carbocation is generally proposed to first undergo cation−alkene cyclization to form a secondary carbocation, the beyeranyl cation (**B**, Scheme 1). **B** is thought to be the precursor of beyerene (**2**) and a key branch point in the reaction pathways leading to kaurene (**3**), trachylobane (**4**), and atiserene (**5**). An alkyl shift (C12 migrating from C16 to C13) in **B** leads to the kauranyl cation (**C**), the precursor to kaurene (**3**). A 1,3-hydride shift in **B** is thought to lead to another secondary cation, **D**, which can form atiserene (**5**) via a subsequent alkyl shift (C13 migrating from C16 to C12) to form cation **E** followed by deprotonation. Alternatively, concerted deprotonation and ring closure of cation **D** could lead to trachylobane (**4**).

In this mechanistic scheme, two secondary carbocation intermediates (**B** and **D**, Scheme 1) are invoked,[2b,6,10] but whether or not these cations are actually viable intermediates is uncertain. Starting with the seminal work of Hess on steroid

(1) (a) Cane, D. E. *Sesquiterpene biosynthesis: cyclization mechanisms*; Elsevier: 1999; Vol. 2, pp 155−200. (b) Cane, D. E. *Chem. Rev.* **1990**, *90*, 1089–1103. (c) Cane, D. E. *Acc. Chem. Res.* **1985**, *18*, 220–226. (d) Christianson, D. W. *Chem. Rev.* **2006**, *106*, 3412–3442. (e) Davis, E. M.; Croteau, R. *Top. Curr. Chem.* **2000**, *209*, 53–95. (f) Christianson, D. W. *Curr. Opin. Chem. Biol.* **2008**, *12*, 141–150.

(2) (a) Hanson, J. R. *Nat. Prod. Rep.* **2007**, *24*, 1332–1341. (b) Roy, A.; Roberts, F. G.; Wilderman, P. R.; Zhou, K.; Peters, R. J.; Coates, R. M. *J. Am. Chem. Soc.* **2007**, *129*, 12453–12460.

(3) Other tetracyclic diterpenes containing bicyclooctane units include aphidicolanol, stemodin, scopadulanol, betaerene, and stemarene, which are generally thought to be derived from *syn*-copalyl diphosphate.[4] These structures will be discussed further in a separate report.

(4) Oikawa, H.; Nakamura, K.; Toshima, H.; Toyomasu, T.; Sassa, T. *J. Am. Chem. Soc.* **2002**, *124*, 9145–9153.

(5) Hong, Y. J.; Tantillo, D. J. *Nat. Chem.* **2009**, *1*, 384–389.

(6) Ravn, M. M.; Coates, R. M.; Flory, J. E.; Peters, R. J.; Croteau, R. *Org. Lett.* **2000**, *2*, 573–576.

(7) (a) Ravn, M. M.; Peters, R. J.; Coates, R. M.; Croteau, R. *J. Am. Chem. Soc.* **2002**, *124*, 6998–7006. (b) Peters, R. J.; Flory, J. E.; Jetter, R.; Ravn, M. M.; Lee, H. J.; Coates, R. M.; Croteau, R. B. *Biochemistry* **2000**, *39*, 15592–15602. (c) Peters, R. J.; Ravn, M. M.; Coates, R. M.; Croteau, R. B. *J. Am. Chem. Soc.* **2001**, *123*, 8974–8978. (d) Peters, R. J.; Croteau, R. B. *Proc. Natl. Acad. Sci. U.S.A.* **2002**, *99*, 580–584. (e) Peters, R. J.; Croteau, R. B. *Biochemistry* **2002**, *41*, 1836–1842. (f) Ravn, M. M.; Coates, R. M.; Jetter, R.; Croteau, R. B. *Chem. Commun.* **1998**, 21–22.

(8) Mander, L. N. *Nat. Prod. Rep.* **2003**, *20*, 49–69.

(9) (a) Coates, R. M.; Cavender, P. L. *J. Am. Chem. Soc.* **2002**, *102*, 6358–6359. (b) Xu, M.; Wilderman, P. R.; Peters, R. J. *Proc. Natl. Acad. Sci. U.S.A.* **2007**, *104*, 7397–7401.

Scheme 1

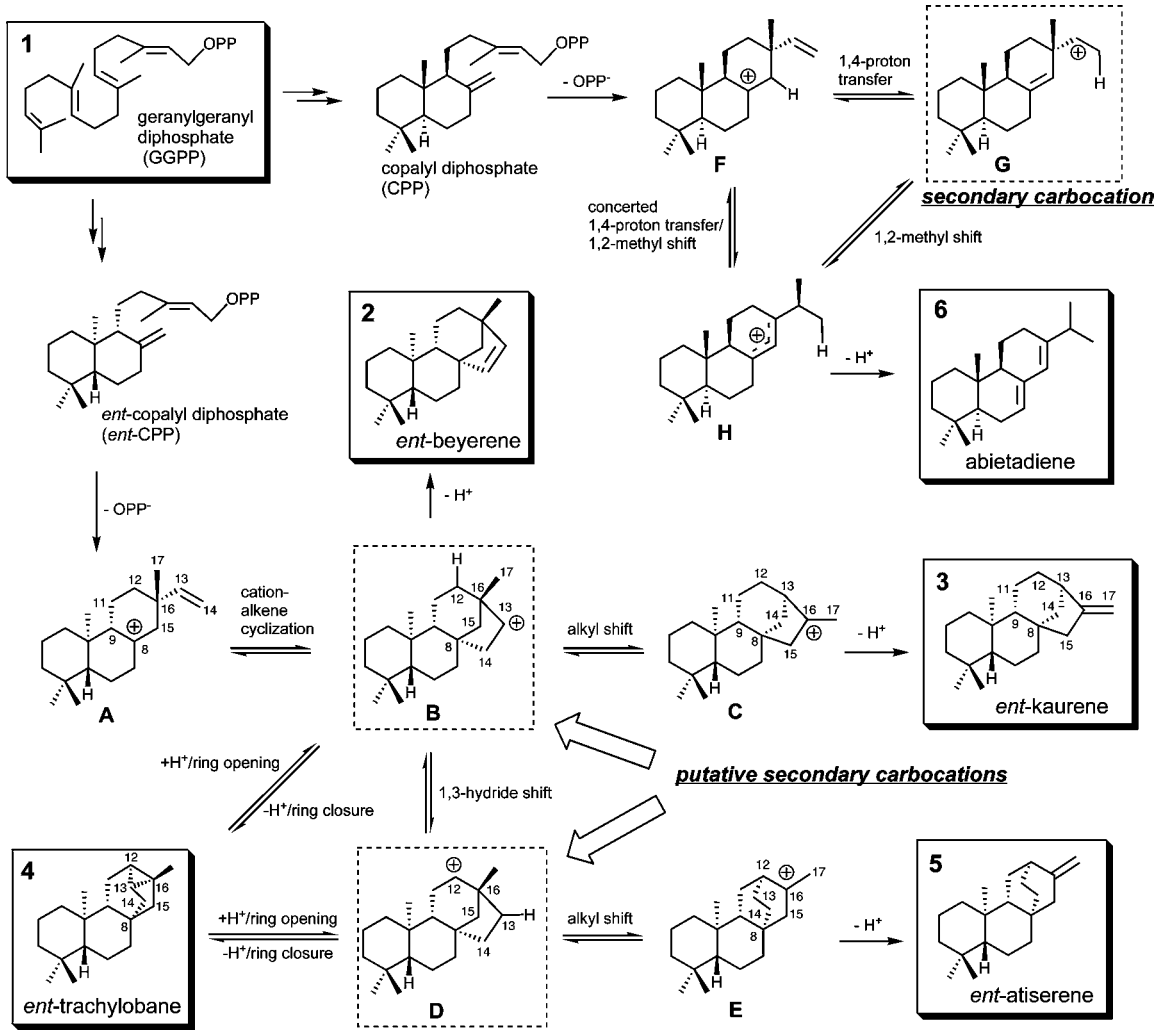

biosynthesis,[11] several studies in which quantum chemical computations were employed to assess the inherent reactivity of other biologically relevant carbocations have shown that secondary carbocations can be avoided by combining two or more mechanistic steps into concerted processes that lead to tertiary carbocations.[11−16] In fact, it has been suggested that proposed secondary carbocations are more often transition state structures than minima, although secondary carbocations are predicted to be true minima in a few cases.[5,14a,17a]

The work described herein extends our theoretical studies on diterpene-forming carbocation cascades.[18] The overall focus of the present study is to investigate the inherent reactivity of carbocations **A**−**E** and to assess how interactions with groups that may be present in diterpene synthase enzymes may modulate this reactivity.

Methods

All calculations were performed with GAUSSIAN03.[19] All geometries were optimized using the B3LYP/6-31+G(d,p) method.[20] All stationary points were characterized by frequency calculations, and reported energies include zero-point energy corrections (unscaled). Intrinsic reaction coordinate (IRC) calculations were used for further characterization of all transition state structures.[21] The B3LYP method is known to perform reasonably well in the prediction of the geometries and behavior of carbo-

(10) (a) Croteau, D.; Vallee, F.; Bergeron, M. G.; LeBel, M. *J. Chromatogr.* **1987**, *419*, 205–212. (b) Vedula, L. S.; Jiang, J.; Zakharian, T.; Cane, D. E.; Christianson, D. W. *Arch. Biochem. Biophys.* **2008**, *469*, 184–194. (c) Seemann, M.; Zhai, G.; de Kraker, J.-W.; Paschall, C. M.; Christianson, D. W.; Cane, D. E. *J. Am. Chem. Soc.* **2002**, *124*, 7681–7689.

(11) (a) Hess, B. A., Jr. *J. Am. Chem. Soc.* **2002**, *124*, 10286–10287. (b) Hess, B. A., Jr. *Org. Lett.* **2003**, *5*, 165–167. (c) For a summary of more recent work from the Hess group, and leading references to the same, see: Hess, B. A., Jr.; Smentek, L. *Collect. Czech. Chem. Commun.* **2008**, *73*, 786–794.

(12) Tantillo, D. J. *J. Phys. Org. Chem.* **2008**, *21*, 561–570.

(13) Lodewyk, M. W.; Gutta, P. G.; Tantillo, D. J. *J. Org. Chem.* **2008**, *73*, 6570–6579.

(14) (a) Hong, Y. J.; Tantillo, D. J. *J. Am. Chem. Soc.* **2009**, *131*, 7999–8015. (b) Hong, Y. J.; Tantillo, D. J. *Org. Lett.* **2006**, *8*, 4601–4604.

(15) Wang, S. C.; Tantillo, D. J. *Org. Lett.* **2008**, *10*, 4827–4830.

(16) (a) Matsuda, S. P. T.; Wilson, W. K.; Xiong, Q. *Org. Biomol. Chem.* **2006**, *4*, 530–543. (b) Rajamani, R.; Gao, J. *J. Am. Chem. Soc.* **2003**, *125*, 12768–12782. (c) Vrcek, V. *Int. J. Quantum Chem.* **2007**, *107*, 1772–1781.

(17) (a) Gutta, P.; Tantillo, D. J. *J. Am. Chem. Soc.* **2006**, *128*, 6172–6179. (b) Gutta, P.; Tantillo, D. J. *Org. Lett.* **2007**, *9*, 1069–1071.

(18) This is part 3 in our series on diterpenes. For parts 1 and 2 and leading references to related work, see refs 5 and 17b.

(19) Frisch, M. J.; et al. *Gaussian03*, revision D.01; Gaussian, Inc.: Pittsburgh, PA, 2003 (full reference in Supporting Information).

(20) (a) Becke, A. D. *J. Chem. Phys.* **1993**, *98*, 5648–5652. (b) Becke, A. D. *J. Chem. Phys.* **1993**, *98*, 1372–1377. (c) Lee, C.; Yang, W.; Parr, R. G. *Phys. Rev. B* **1988**, *37*, 785–789. (d) Stephens, P. J.; Devlin, F. J.; Chabalowski, C. F.; Frisch, M. J. *J. Phys. Chem.* **1994**, *98*, 11623–11627.

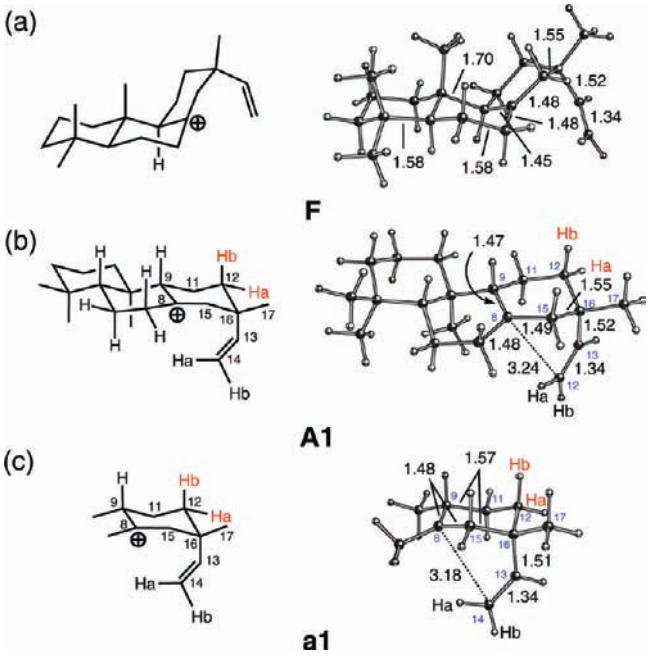

Figure 1. Computed geometries (distances in Å) of reference structures **F**, **A1**, and **a1**. See Methods section for details.

cations.[5,12−17,22−26] We also include mPW1PW91/6-31+G(d,p)//B3LYP/6-31+G(d,p) energies for comparison, based on a suggestion by Matsuda and co-workers, who showed that B3LYP likely underestimates the relative energies of cyclic structures versus acyclic isomers.[16a] These energies include unscaled zero-point energy corrections from B3LYP/6-31+G(d,p) frequency calculations. We have used these methods previously to study other terpene-forming carbocation rearrangement reactions (and have compared them to the results of other methods).[5,13−15,17,23−26] All energies for intermediates and transition state structures in this report are relative to that of structure **F** for the full system (Figure 1a)[5] and **a1** for the small model system (Figure 1c). Structure **F** is used here as a reference so that the energies described herein can be compared directly to those reported in ref 5 for isomeric carbocations. The energy of structure **A1** (Figure 1b), which is a diastereomer of **F** (differing in the absolute configuration of most stereocenters and also in terms of conformation), is actually less than 0.3 kcal/mol different than that of **F** (see Figure 2). Structure **a1** is a model of **A1** that bears only one cyclohexane ring (*vide infra*). Structural drawings were produced using the *Ball & Stick* program.[27] Throughout the manuscript, bold numbers are used to label neutral molecules, primed numbers are used for corresponding small models, and letters (capital letters for full systems and lower case letters for small models) are used to label carbocation intermediates. Numbers following letters for carbocations are used to label different conformations. Atom numbering indicated in the structures in this report refers to that of kaurene (**3**, Scheme 1). To facilitate comparison, the same atom numbering is employed for the small model system, even though it contains many fewer atoms.

Results and Discussion

Formation of Kaurene (3). Our investigation begins with a pathway to kaurene from a conformer of the pimarenyl cation (**A**, Scheme 1) that is productive for the proposed cyclization to form **B**. Computed reaction pathways from this conformer,

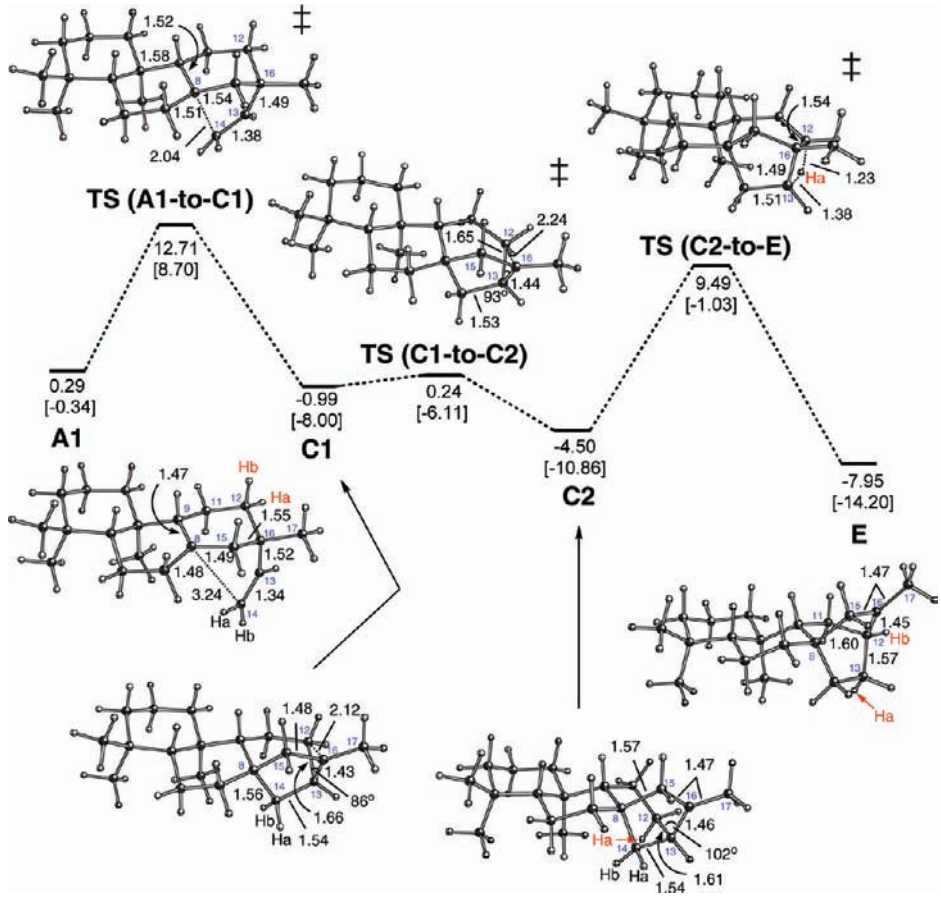

Figure 2. Computed rearrangement of **A1**. Computed geometries (distances in Å) and relative energies (kcal/mol) of intermediates and transition state structures are shown; B3LYP/6-31+G(d,p)//B3LYP/6-31+G(d,p) in normal type and mPW1PW91/6-31+G(d,p)//B3LYP/6-31+G(d,p) in brackets (see Methods section for details).

Scheme 2

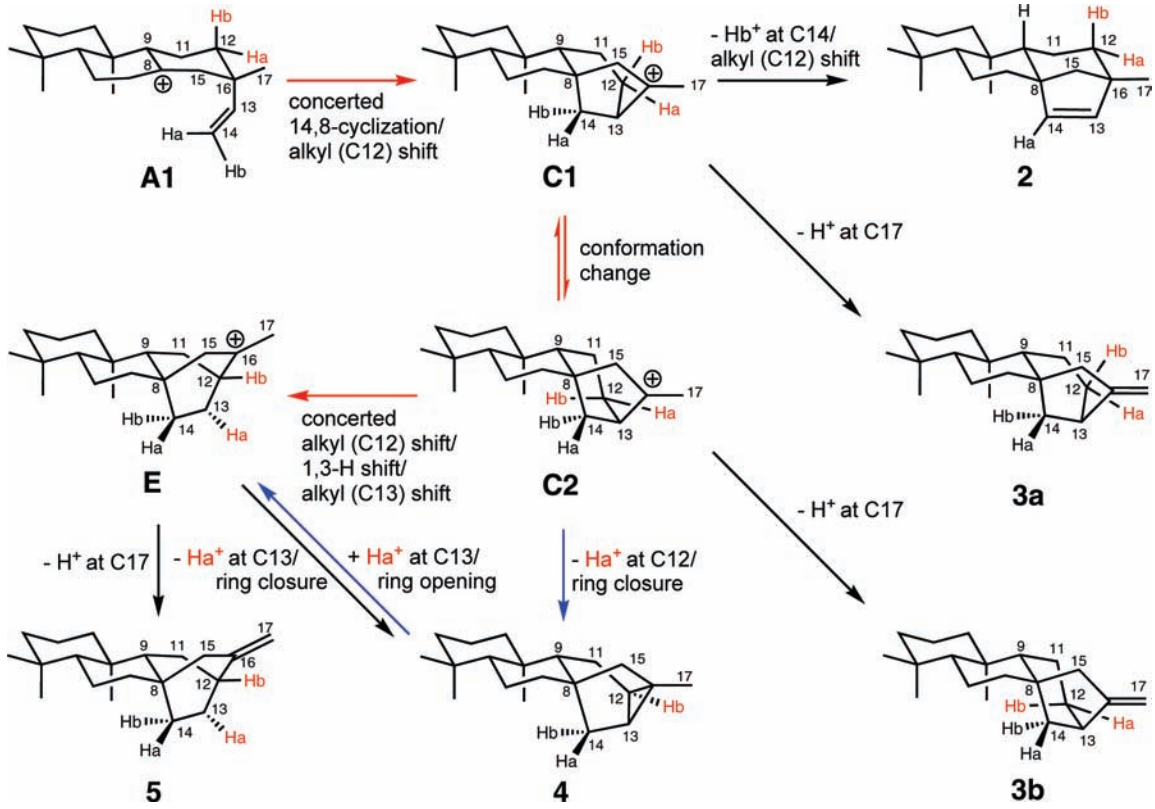

A1, and geometries of structures involved in these pathways are shown in Scheme 2 and Figure 2. The first step in the proposed mechanism is cation-alkene cyclization via attack of the C13═C14 π-bond of **A1** on C8. This reaction would generate the putative secondary cation **B** (Scheme 1). We were able to locate a transition state structure that resembles the expected transition state structure for cyclization of **A1** (Figure 2), but IRC calculations suggested that this transition state structure actually connects **A1** to **C1** via a concerted process with asynchronous cyclization and alkyl shifting (C12 from C16 to C13) events (Figure 3).[12] Although the formation of the proposed secondary carbocation **B** as a minimum thus appears to be avoided, structures resembling cation **B** appear on the righthand shoulder of the pathway connecting the transition state structure to **C1** (Figure 3). The **A1**→**C1** transformation is somewhat analogous to a rearrangement of the bisabolyl cation involved in the formation of trichodiene, in which a concerted cyclization/methyl shift reaction also allows the system to avoid a secondary cation.[12,14b,26] In the structure of **C1** (Figures 2 and 3), the C13−C16 bond is only 1.43 Å long, while the C12−C13 bond is significantly elongated to 1.66 Å, consistent with strong hyperconjugation of the C12−C13 σ-bond with cationic center C16. Carbocation **C1** actually resides on the verge of C12 bridging, in the middle ground of the classical/nonclassical continuum (note that the C16−C13−C12 angle is only 86°).[28,29] Direct deprotonation from the C17 methyl group of cation **C1** would generate kaurene (as conformer **3a**, Scheme 2; computed geometries and relative energies of diterpene products are included in the Supporting Information). Alternatively, water capture at C16 would generate the diterpene alcohol kauranol.[30]

Formation of Atiserene (5). Atiserene (**5**) is expected to be derived from **E**, which is hypothetically formed from **B** via **D**, by deprotonation (Scheme 1), but as mentioned above, we were not able to locate a secondary cation corresponding to **B** as a minimum. Nevertheless, we were able to locate a transition state structure that initially appeared to be a transition state structure for a 1,3-hydride transfer connecting hypothetical secondary cations **B** and **D** (Figure 2, right). Surprisingly, subsequent IRC calculations (see Figure 4) indicated that this transition state structure is actually connected to **C2** (another conformer of cation **C**, connected to **C1** by a small barrier) and **E** (Scheme 2 and Figure 2). The **C2**→**E** conversion is predicted to be a concerted reaction in which *three* events—alkyl (C12) shift, 1,3-hydride shift, and alkyl (C13) shift—occur asynchronously (Figure 4). Initial changes in the **C2** geometry along the IRC path involve C12−C13 bond breaking and C12−C16 bond forming events, which again generate transient structures similar

(21) (a) Gonzalez, C.; Schlegel, H. B. *J. Phys. Chem.* **1990**, *94*, 5523–5527. (b) Fukui, K. *Acc. Chem. Res.* **1981**, *14*, 363–368.
(22) Hong, Y. J.; Tantillo, D. J. *J. Org. Chem.* **2007**, *72*, 8877–8881.
(23) Gutta, P.; Tantillo, D. J. *Angew. Chem., Int. Ed.* **2005**, *44*, 2719–2723.
(24) Bojin, M. D.; Tantillo, D. J. *J. Phys. Chem. A* **2006**, *110*, 4810–4816.
(25) Ho, G. A.; Nouri, D. H.; Tantillo, D. J. *J. Org. Chem.* **2005**, *70*, 5139–5143.
(26) Hong, Y. J.; Tantillo, D. J. *Org. Biomol. Chem.* **2009**, *7*, 4101–4109.
(27) Müller, N.; Falk, A.; Gsaller, G. *Ball & Stick V.4.0a12, molecular graphics application for MacOS computers*; Johannes Kepler University, Linz, Austria, 2004.
(28) For leading references, see: (a) Grob, C. A. *Acc. Chem. Res.* **1983**, *16*, 426–431. (b) Brown, H. C. *Acc. Chem. Res.* **1983**, *16*, 432–440. (c) Olah, G. A.; Prakash, G. K. S.; Saunders, M. *Acc. Chem. Res.* **1983**, *16*, 440–448. (d) Walling, C. *Acc. Chem. Res.* **1983**, *16*, 448–454. (e) Brown, H. C. (with comments by Schleyer, P. v. R.) *The Nonclassical Ion Problem*; Plenum: New York, 1977.
(29) Tantillo, D. J. *Chem. Soc. Rev.*, submitted.
(30) Morris, B. D.; Foster, S. P.; Grugel, S.; Charlet, L. D. *J. Chem. Ecol.* **2005**, *31*, 89–102.

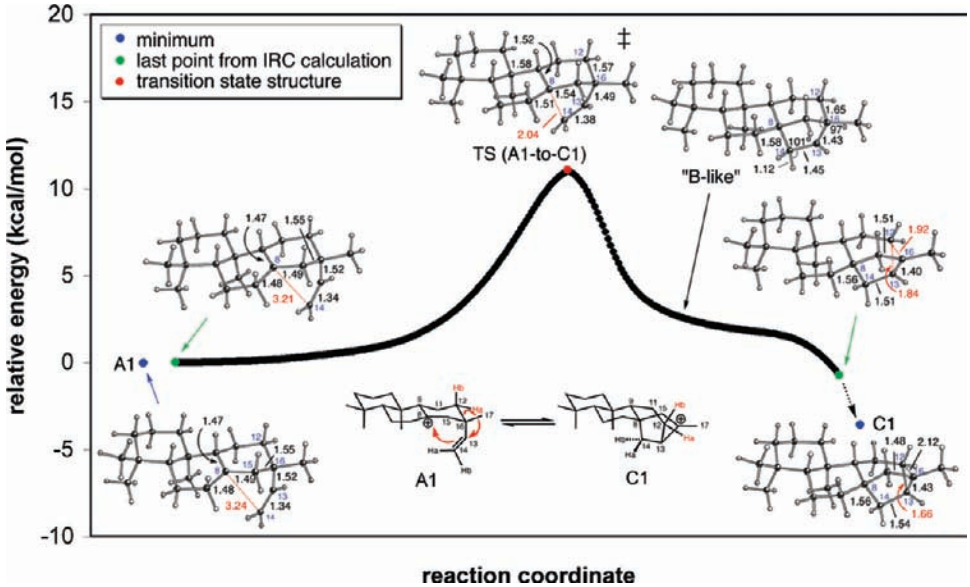

Figure 3. Conversion of **A1** to **C1** from IRC calculations (B3LYP/6-31+G(d,p); energies do not include zero-point energy corrections).

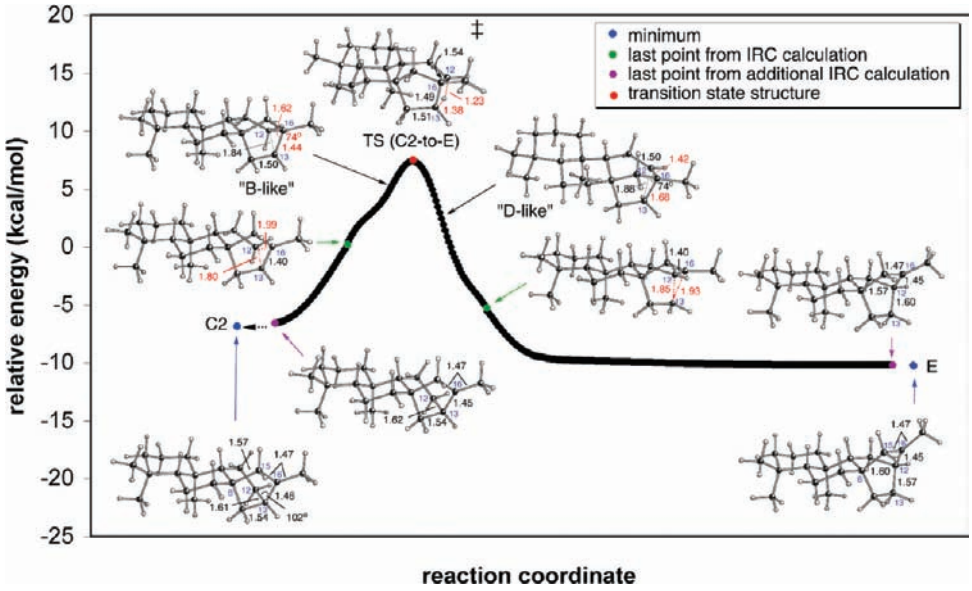

Figure 4. Conversion of **C2** to **E** from IRC calculations (B3LYP/6-31+G(d,p); energies do not include zero-point energy corrections). The initial IRC calculation toward **C2** (run using "calcfc") stopped at the point indicated in green at the left (geometry shown) due to a convergence problem. Note that the geometry at this point already shows significant alkyl shifting. To further verify the connection of **TS** (**C2-to-E**) to **C2**, an additional IRC calculation was carried out using the wavefunction and geometry from the last point of the first IRC calculation and recalculating the force constants (i.e., using "calcfc"); this led to the structure at the left corresponding to the purple point on the plot. The same procedure was used for the (**C2-to-E**)-to-**E** portion of the reaction.

to the hypothetical secondary cation **B** (Figure 4, left). These changes shift the cationic center from C16 to C13 and prepare the geometry for a hydride transfer (of, specifically, hydrogen H_a shown in red) from C12 to C13. Transient structures similar to hypothetical secondary cation **D** appear after the hydride transfer (Figure 4, right), however C13−C16 bond breaking and C12−C13 bond formation following hydride transfer lead directly to the tertiary cation **E**. This sequence of events is illustrated in Scheme 3; it is important to note, however, that the two secondary cation structures shown (**B** and **D**) are not discrete minima on the potential energy surface.[31] The barrier for the **C2**→**E** reaction is computed to be ∼10−14 kcal/mol from **C2** (Figure 2). This process again allows the system to avoid secondary cations (**B** and **D**) as minima.[3,4,11−16,29,32] Overall, the **A1**→**E** pathway is significantly exothermic (by ∼8−14 kcal/mol; Figure 2). Direct deprotonation from C17 of **C2** would also generate kaurene (as conformer **3b**, Scheme 2), and water capture at C16 would generate kauranol. Direct deprotonation from C17 of **E** would lead to atiserene (**5**; Schemes 1 and 2), while water capture at C16 of **E** would generate the diterpene alcohol atiseranol.[30]

Formation of Trachylobane (4). Wanting to expand our study to many additional rearrangement pathways, and noting that the two cyclohexane rings appear to play mainly a spectator role

(31) A related rearrangement has been observed previously. See ref 26.

(32) Hong, Y. J.; Tantillo, D. J. Unpublished results on other systems.

Scheme 3

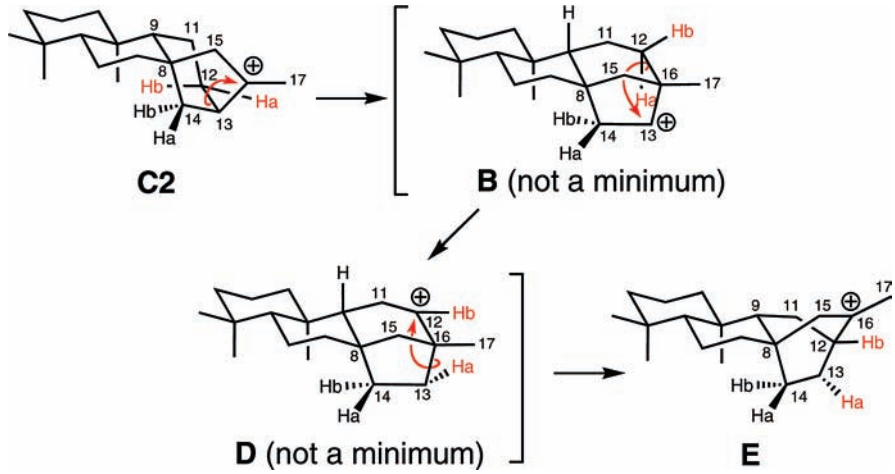

in the rearrangements described above, we explored whether a small, less computationally demanding, model system could be used. As shown in Figure 5 (box), upon replacing the trimethyl decalin unit with two methyl groups, a qualitatively similar energy surface is found (compare with Scheme 2 and Figure 2; see Supporting Information for geometries). We used this small model system to explore the formation of trachylobane (**4**, Scheme 1). Trachylobane could be derived from **B** by deprotonation (from C12) and ring closure (C12−C13 σ-bond formation) in a concerted fashion (Scheme 1), but as described above, cation **B** was not found as a minimum. We were able to locate a transition state structure, using ammonia as a model

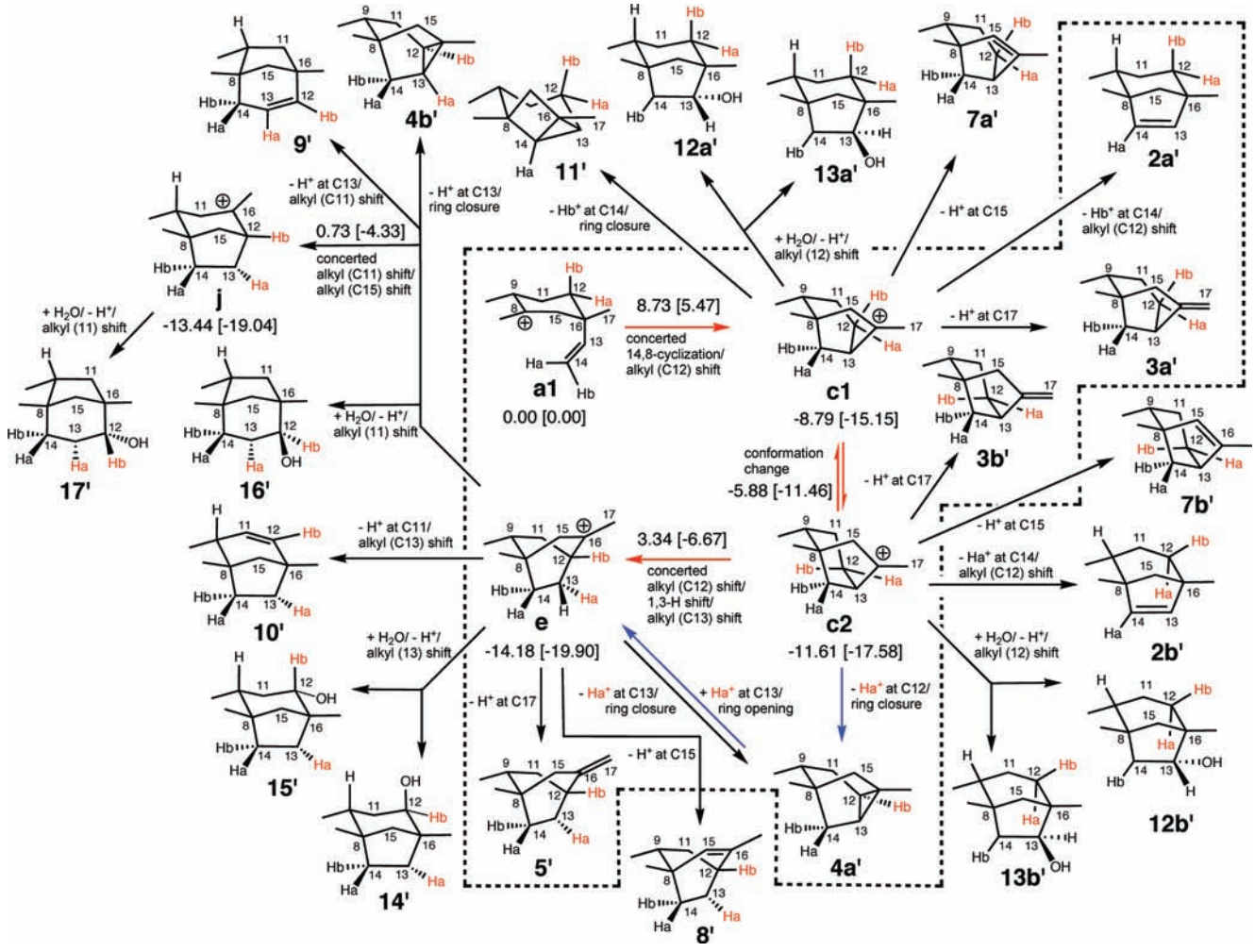

Figure 5. Computed rearrangements and quenching reactions for **a1**. Computed energies (in kcal/mol) of intermediates and transition state structures are shown; B3LYP/6-31+G(d,p)//B3LYP/6-31+G(d,p) in normal type and mPW1PW91/6-31+G(d,p)//B3LYP/6-31+G(d,p) in brackets (see Methods section for details). Structures in the dashed box correspond to small models of those shown in Scheme 2. Some of the reactions shown are not discussed in the text but are described in the Supporting Information.

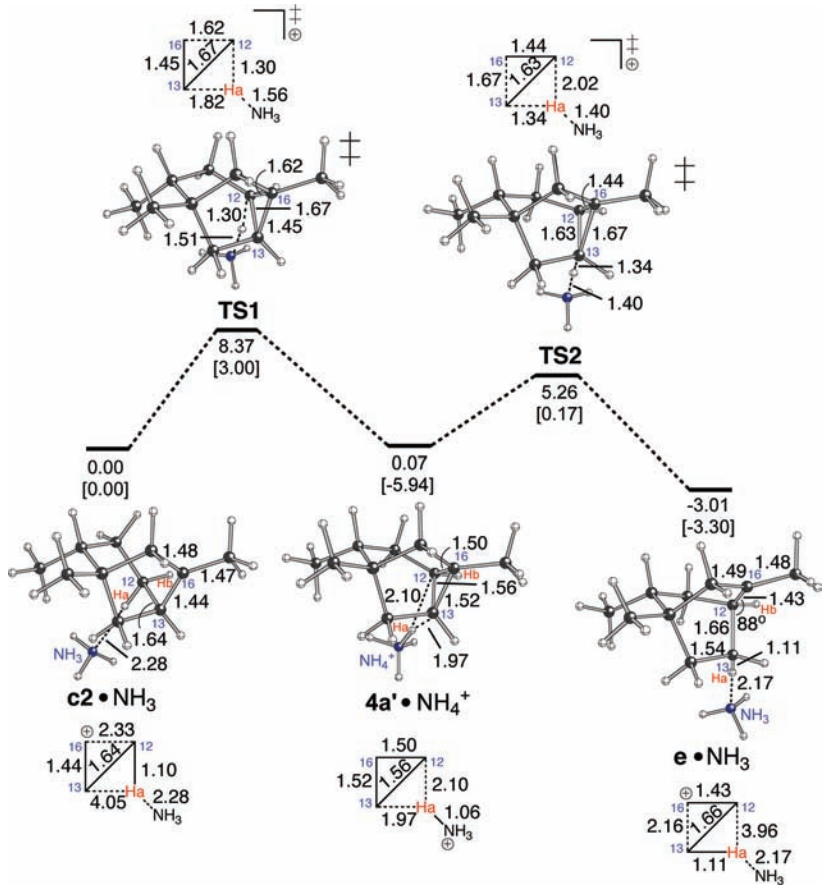

Figure 6. Model for **C2**→**E** interconversion via a deprotonation/reprotonation mechanism. Computed structures (distances in Å) and relative energies (kcal/mol, relative to the energy of the **c2**•NH_3 complex) of intermediates and transition state structures are shown; B3LYP/6-31+G(d,p)//B3LYP/6-31+G(d,p) in normal type and mPW1PW91/6-31+G(d,p)//B3LYP/6-31+G(d,p) in brackets (see Methods section for details).

base,[13,14a,22,24,32,33] that looks like what one would expect for such a process (Figure 6, **TS1**; note that it is the proton *syn* to the forming bond, H_a, that is transferred), but IRC calculations (see Supporting Information) indicated that this transition state structure actually connects an ammonia complex of cation **c2** (held together by a C−H···N interaction[22,24]) to a complex of **4′** with an ammonium cation. The computed barrier for this conversion is <10 kcal/mol. A similar process was described for the formation of the sesquiterpene cyclosativene.[13] Ammonia is used here as a model base because it is simple (symmetrical, small) and well-behaved computationally. Although lysine residues are generally not found in terpene synthase active sites, residues such as histidine are.[1d] Still, we do not intend to imply that something as basic as an amine is necessary to play the role adopted by ammonia in our calculations, but instead intend to show the sorts of structural distortions that are possible when C−H···X interactions are present and the types of rearrangements that can be coupled to deprotonation events. We have previously examined other electron-rich active site residue models—benzene as a model of phenylalanine and tyrosine,[22] water[14a] (*vide infra*)—and continue to explore others.[32]

We also located an analogous transition state structure for concerted deprotonation/ring closure (C13−C16 σ-bond formation) of cation **e** with a comparable barrier (Figure 6; see Supporting Information for a discussion of alternative deprotonations of **E**/**e** that could also lead to trachylobane or to other diterpenes). Thus, we predict that trachylobane could be formed directly from **C2** or **E**. Note that these calculations suggest that **C2** and **E** could also be interconverted via a stepwise deprotonation/reprotonation process (**C2**→**4**→**E**) with a low barrier. Although a two-step proton transfer process via trachylobane (**4**) has been suggested in the literature,[2b] we suggest that such a process would interconvert cations **C2** and **E** rather than cations **B** and **D**.

Formation of Beyerene (2). Beyerene (**2**) could also have been derived from secondary cation **B** by direct deprotonation (Scheme 1) if **B** existed as an intermediate. Instead, we located a transition state structure connecting an ammonia complex of cation **c1** to a complex of **2a′**, our small model of beyerene, with an ammonium cation (Figure 7) via a concerted alkyl shift/deprotonation (C12 migrating between C13 and C16) reaction.[34] The IRC from **TS3** is quite interesting (Figure 8). While the pathway toward the **2a′**•NH_4^+ product complex is sharply downhill, as expected, the pathway back toward the **c1**•NH_3 complex is rather flat. Full optimizations of the structures in the flat region of the IRC consistently lead to the **c1**•NH_3

(33) Complexation with ammonia at C12-H_a and C13-H_a brings subtle geometrical changes to **c2** and **e**, respectively, suggesting that these cations are perhaps somewhat malleable. Similar geometric changeability has been described for the behavior of the 2-norbornyl cation. See ref 22.

(34) We also located a transition state structure connecting an ammonia complex of cation **c2** to an ammonium complex of our small model of beyerene with a boat-like conformation of the six-membered ring via another concerted alkyl shift/deprotonation (C12 migrating between C13 and C16) reaction. See Supporting Information for details on this and other deprotonation reactions of **c1** and **c2**.

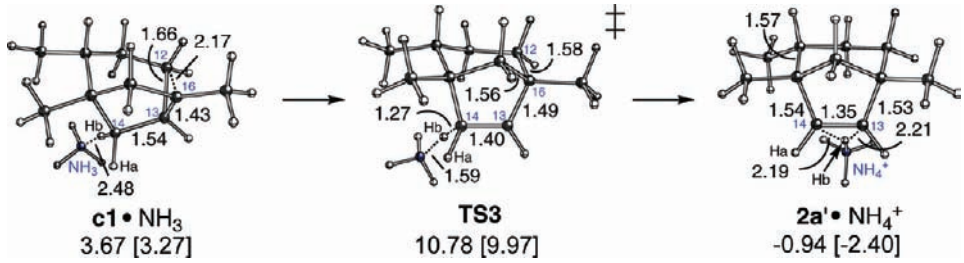

Figure 7. Models for deprotonation to form beyerene (**2**). Computed structures (distances in Å) and energies (kcal/mol, relative to that of the **c2**•NH_3 complex in Figure 6) of intermediates and transition state structures are shown; B3LYP/6-31+G(d,p)//B3LYP/6-31+G(d,p) in normal type and mPW1PW91/6-31+G(d,p)//B3LYP/6-31+G(d,p) in brackets.

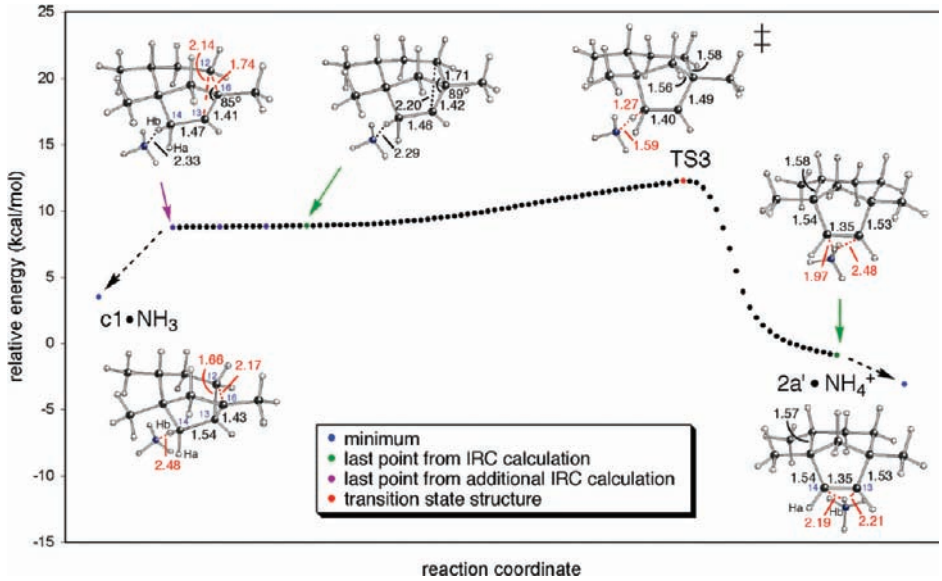

Figure 8. Conversion of **c1** to **2a′** from IRC calculations (B3LYP/6-31+G(d,p); energies do not include zero-point energy corrections). The initial IRC calculation toward the **c1**•NH_3 complex (run using "calcfc") stopped at the point indicated in green at the left (geometry shown). Three consecutive additional IRC calculations were then carried out, each using the wavefunction, geometry, and force constants from the last point of the previous IRC calculation (i.e., using "rcfc").

complex. Still, the plateau region contains some structures with secondary cation-like geometries.[35−37]

Formation of Diterpene Alcohols. We also explored the possibility of forming alcohols **12**−**15**, which could, in principle, be formed from secondary carbocations via direct water capture (Figure 9).[38] Transition state structures connecting carbocation• water complexes with models of protonated **12** and **13** were located (Scheme 4 and Figure 10). Attack of water on C13 from the righthand side of **c1** (as drawn; Scheme 4a and Figure 10a) is predicted to be accompanied by a shift of C12 from C13 to C16, leading to **12′**-H^+. This process, although concerted, was actually quite asynchronous,[12] however, with the alkyl shift event largely preceding C−O bond formation. We also located a transition state structure that appears to connect a water complex of secondary cation **b** with **13′**-H^+ (**TS5**; Scheme 4b and Figure 10b). This transition state structure is indeed connected to a water complex of cation **b**, in which the water molecule interacts directly with the p-like orbital at C13 (at an O···C distance of 2.65 Å). Thus, although cation **b** does not exist as a minimum in the gas phase, it does in the presence of an appropriately oriented water molecule (see the Supporting Information for a related **B**•NH_3 complex).

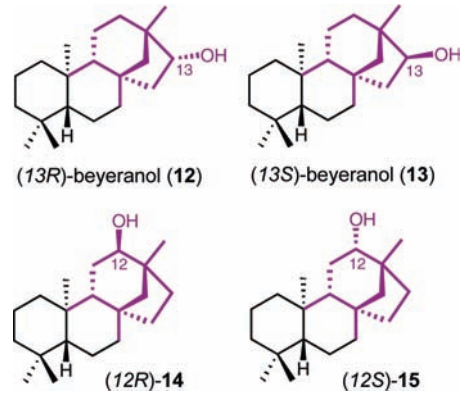

Figure 9. Structures of diterpene secondary alcohols (**12**−**15**), with the portion of each molecule that is included in our small model systems highlighted.

(35) In some cases, bifurcations have been suggested to occur near plateau regions of reaction coordinates (e.g., Nouri, D. H.; Tantillo, D. J. *J. Org. Chem.* **2006**, *71*, 3686–3695, and ref 5), but we were not able to find a transition state structure in the plateau region shown in Figure 8.

(36) We also explored the possibility of a [1,2]-hydride shift between C13 and C14 of **c1**. See Supporting Information for details.

(37) See Supporting Information for calculations on an alternative deprotonation of **C1**/**c1** that could lead to an unusual diterpene with a strained housane (bicyclo[2.1.0]pentane) substructure.

(38) See Supporting Information for additional calculations on the formation of related secondary alcohols containing bicyclo[3.2.1]octane substructures (modeled using systems **16′** and **17′** in Figure 5).

Scheme 4

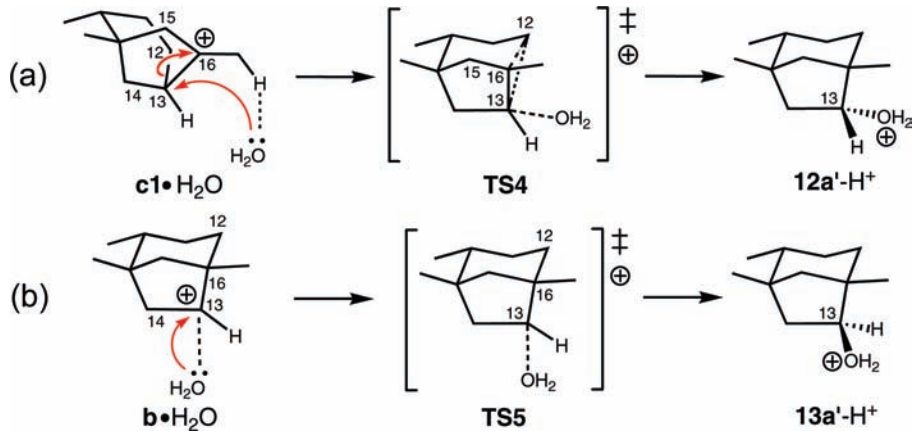

Scheme 5

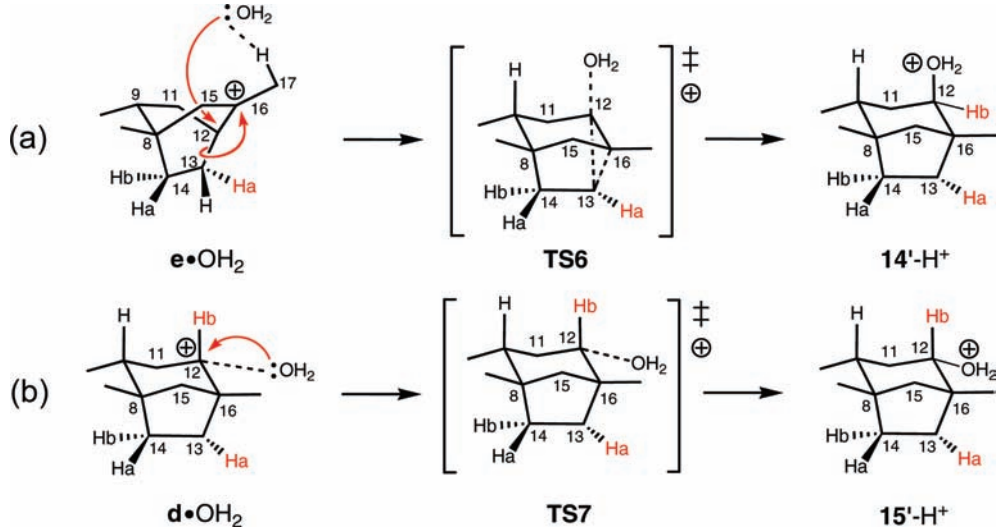

Alcohols **14** and **15** could be formed from secondary carbocation **D**, if it existed as a minimum, via water capture at C12. We located transition state structures that appear to correspond to water addition to cation **d** to form **14′**-H^+ and **15′**-H^+ (Scheme 5 and Figure 11). Although the transition state structure for formation of **14′**-H^+ (**TS6**; Scheme 5a and Figure 11a) is connected to a water complex of cation **e**, thereby allowing secondary cation **d** to be avoided, the transition state structure for formation of **15′**-H^+ (**TS7**; Scheme 5b and Figure 11b) is connected to a water complex of secondary cation **d**. In this complex, the water molecule interacts directly with the p-like orbital at C12 (at an O···C distance of 2.46 Å). Thus, these results suggest that the nature of both cations **B** and **D** most likely depends on the nature of the environment in which they are formed, akin to cations preceding the sesquitheriferol sesquiterpenes (**18** and **19**).[14a] It makes sense that the reactions that lead to **14′** and **15′** mirror those that form **18** and **19** in that the bridged bicyclic cores of **14**/**15** and **18**/**19** are the same (enantiomers, actually; Chart 1).

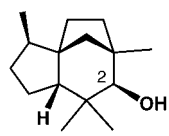

(2*S*)-sesquithuriferol (**18**)

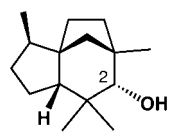

(2*R*)-sesquithuriferol (**19**)

Chart 1

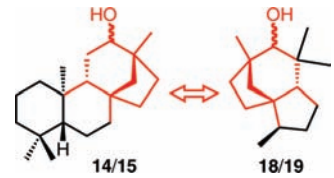

Implications. (1) Are Secondary Carbocations Avoided? We suggest that the previously proposed mechanisms shown in Scheme 1 should be modified. Secondary carbocations **B** and **D** are generally not found as minima (except in specific types of scenarios; see point (2) below), and so we propose that the central carbocations that spawn diterpenes **2**−**5** by deprotonation are likely tertiary carbocations **C** and **E** (Scheme 2) in most scenarios.

(2) Means of Avoidance. As observed in scattered previous studies on the formation of both smaller[13−15] and larger[11,16] terpenes, secondary carbocations are avoided by combining two or more putative reaction steps into a concerted process.[5,12,29] Of particular note for the systems described herein is the triple (1,2-alkyl/1,3-hydride/1,2-alkyl) shift shown in Scheme 3 and Figure 4 and the variety of processes coupled to termination steps (deprotonation and water addition; see Figure 5).[39] The termination reactions described herein demonstrate that when an active site base or nucleophile is appropriately positioned,

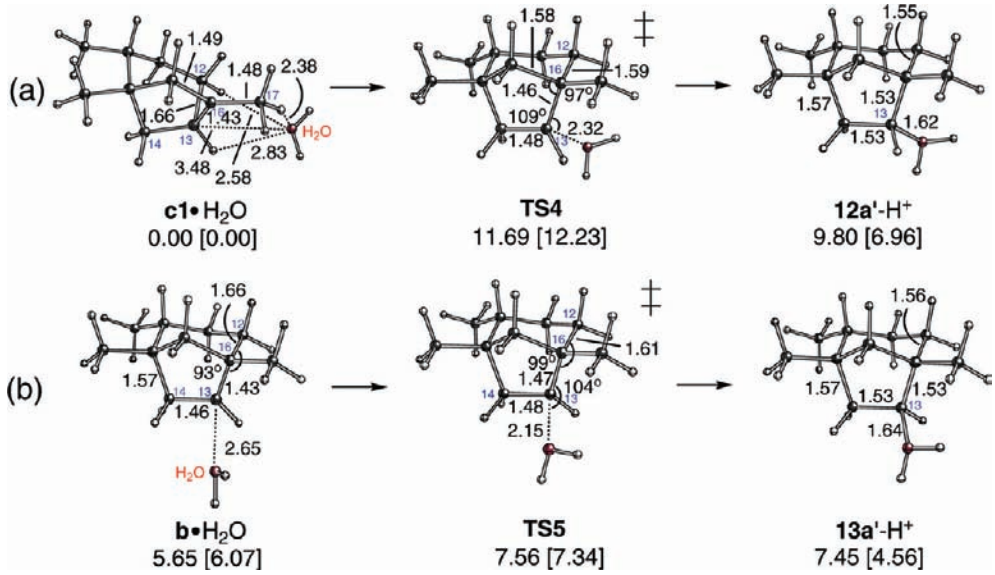

Figure 10. Water•**c1** and water•**b** complexes, transition state structures for water addition, and protonated product alcohols; (a) and (b) show complexation and water addition to different faces of C13. Selected distances are shown in Å. Computed relative energies in kcal/mol (relative to the energy of complex **c1**•H_2O in (a)) are from B3LYP/6-31+G(d,p)//B3LYP/6-31+G(d,p) and mPW1PW91/6-31+G(d,p)//B3LYP/6-31+G(d,p) calculations (normal text and text in brackets, respectively).

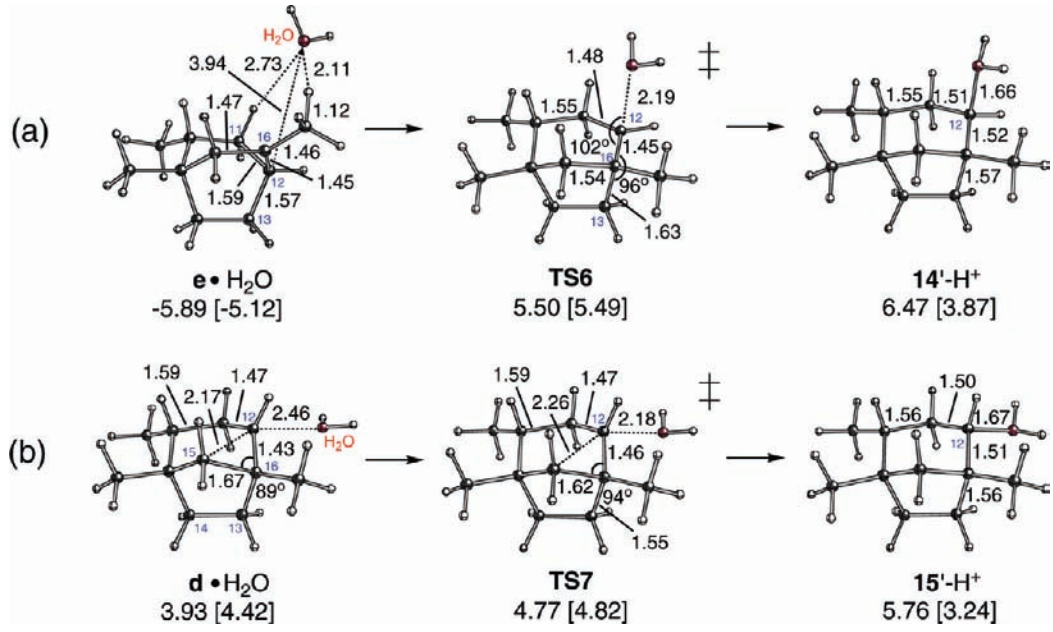

Figure 11. Water•**d** and water•**e** complexes, transition state structures for water addition, and protonated product alcohols (**14**−**15**); (a) and (b) show complexation and water addition to different faces of C12. Selected distances are shown in Å. Computed relative energies in kcal/mol (relative to the energy of complex **c1**•H_2O in Figure 10a) are from B3LYP/6-31+G(d,p)//B3LYP/6-31+G(d,p) and mPW1PW91/6-31+G(d,p)//B3LYP/6-31+G(d,p) calculations (normal text and text in brackets, respectively).

and orbitals in a carbocation are appropriately aligned (which can be controlled in some cases by biasing the system toward a particular conformation), it is possible to form a product with a significantly different molecular architecture than its precursor. Occasionally, such positioning actually allows a secondary carbocation to exist as a minimum (Figures 10−11).

(3) Cation Mimicry. Ammonium cations **20**−**21** were used in previous experimental studies as aza-analogs of putative carbocation **B** and a corner protonated (at C13) trachylobane (which the authors suggested could be an intermediate or transition state structure).[2b] As discussed above, **B** is not found to be a minimum in the gas phase, but **B** can exist as a minimum when complexed with water (Figure 10b). The transition state structure for deprotonation to form beyerene (**TS3**, Figures 7−8) actually resembles the proposed structure of **B**/**b**

(39) The triple shift reaction also sheds light on the pathways to diterpenes derived from *syn*-CPP,[3] studied previously by Oikawa and co-workers, using density functional calculations coupled to experiments.[4] These authors suggested that the secondary carbocations generally proposed in mechanisms leading to these diterpenes are actually transition state structures.[4] However, it was not stated clearly which intermediates are actually connected via those transition state structures. In particular, a transition state structure for 1,3-hydride shift is shown connected to two other transition state structures. By analogy to our results, we suggest that the results described in ref 4 are readily rationalized by invoking a concerted triple shift mechanism. Detailed calculations on these systems will be reported in due course.

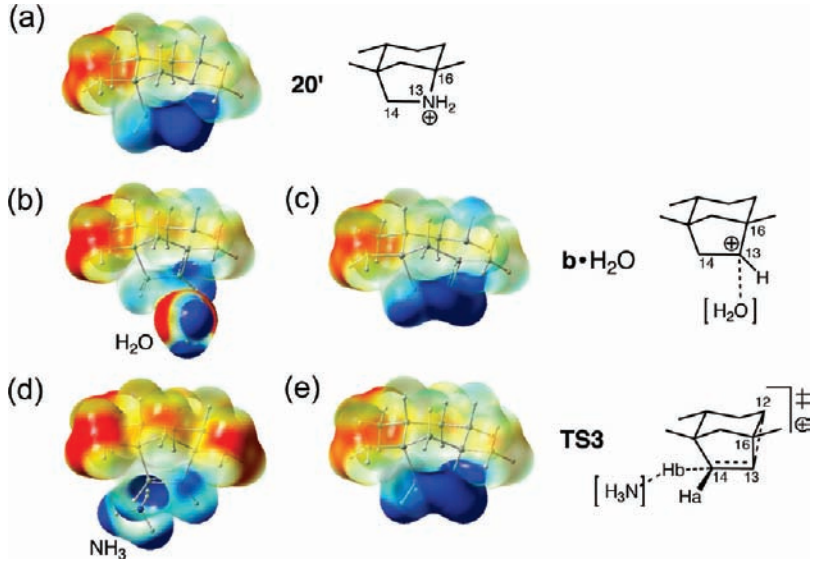

Figure 12. Electrostatic potential surfaces (B3LYP/6-31+G(d,p)) for (a) **20′**, (b) water•**b** complex, (c) water•**b** complex with the H_2O fragment deleted, (d) **TS3**, and (e) **TS3** with the NH_3 fragment deleted. Red is least positive and blue is most positive; the range is +0.135 to +0.240 au.

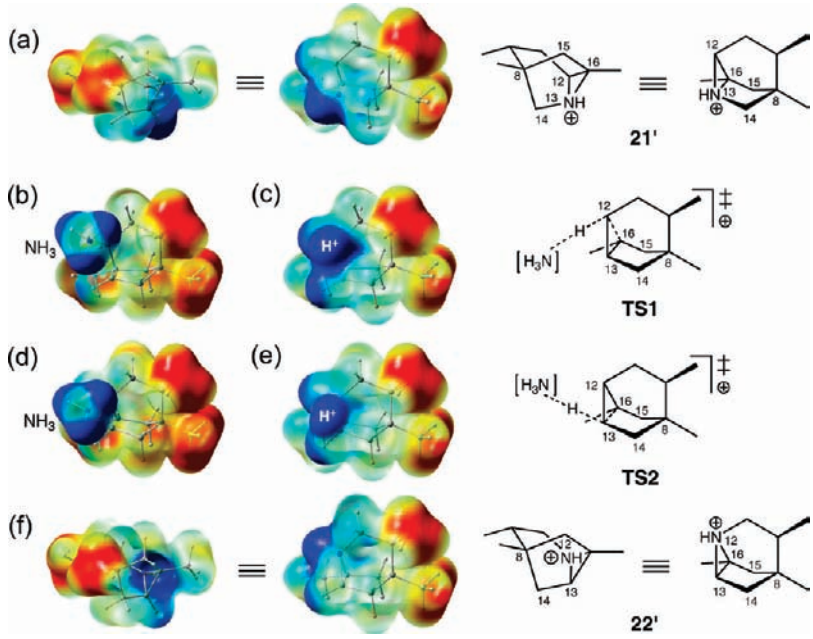

Figure 13. Electrostatic potential surface for (a) **21′**, (b) **TS1**, (c) **TS1** with the NH_3 fragment deleted, (d) **TS2**, (e) **TS2** with the NH_3 fragment deleted, and (f) **22′**. Red is least positive and blue is most positive; the range is +0.135 to +0.240 au.

and the hydrocarbon portion of the water−**b** complex. Consequently, we suggest that ammonium ion **20** actually mimics either transition state structure **TS3** or a complex of **B** with water (or perhaps diphosphate). This contention is further supported by a comparison of electrostatic potential maps computed for **20′** (a truncated model of **20**), the **b**•H_2O complex, and **TS3** (Figure 12).

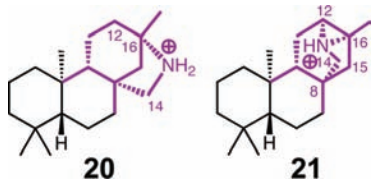

Moreover, based on our calculations, **21** appears to mimic transition state structures for protonation of **4′** (**TS1** and **TS2**, Figure 6), rather than an intermediate or a transition state structure for a 1,2-alkyl shift (**B**→**C** or **D**→**E**). This proposal is again supported by electrostatic potential surface calculations (Figure 13a−e). We also propose that an alternative aziridinium ion, **22**, could serve as a mimic of these transition state structures (Figure 13f).

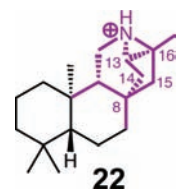

Conclusion

Overall, our calculations on the pathways shown in Figure 1 have led us to propose significant changes to these mechanisms to avoid the intermediacy of secondary carbocations. In some

cases, this is accomplished via complex rearrangements such as the triple shift rearrangement shown in Scheme 3 and Figure 4 or by coupling alkyl shifts to deprotonation events. We hope that our new mechanistic proposals will help to shape future experimental studies on these fascinating rearrangements, such as tests of the computationally predicted stereochemical outcomes for various rearrangements.

Acknowledgment. We gratefully acknowledge UC Davis, the National Science Foundation's CAREER program (CHE-0449845), and the National Science Foundation's Partnership for Advanced Computational Infrastructure (CHE-030089; Pittsburgh Supercomputer Center) for support. We thank Mike Lodewyk for helpful comments.

Supporting Information Available: Coordinates and energies for all computed structures, complete ref 19, and information on calculations not described in detail in the text. This material is available free of charge via the Internet at http://pubs.acs.org.

JA9084786